

Review Article

phys. stat. sol. (a) **2**, 7 (1970)

Subject classification: 12; 1.3; 2; 22.1.2; 22.6

School of Physics, University of New South Wales, Kensington

Cone Crack Closure in Brittle Solids

By

J. S. WILLIAMS, B. R. LAWN, and M. V. SWAIN

Contents

1. Introduction

2. Theoretical crack closure and healing models

3. Optical observations of cone fracture in glass

- 3.1 Observations with polarized light
- 3.2 Observations with critically reflected light
- 3.3 Closure prevention mechanism

4. X-ray topographical studies in silicon

- 4.1 X-ray topography of cracked specimens
- 4.2 X-ray mismatch fringe patterns
- 4.3 Closure prevention mechanism

5. Conclusion

References

1. Introduction

Studies of the opening and closing of crack interfaces during the cyclic loading and unloading of brittle test specimens are of interest because they reveal something of the irreversible processes that occur in the fracture of brittle solids. Such information has an important bearing on a number of related fields. Most directly, it relates to the mechanical strength of a solid, an imperfectly closed crack representing a source of potential weakness. Such is the case, for instance, when minute abrading particles open up microcracks on an otherwise undamaged brittle specimen surface [1]: the microcracks fail to close in perfect registry and thereby lead to a reduction in the breaking stress of the specimen. A useful practical application of this observation is to certain types of fracture testing, in which a careful abrasion of test specimens provides a means for accurately controlling breaking strength parameters [2, 3]. Irreversible processes also determine to a large extent the mechanical properties of a solid cleaved in the presence of an ambient medium. The fracture of mica [4 to 6] and glass [2, 7] is certainly strongly environment-sensitive, particularly with respect to

the presence of water vapour. The mechanism by which the environmental agent penetrates to the crack tip, thus directly influencing crack propagation, is not well understood, but a full explanation would appear to involve the geometrical configuration of the open crack interface. Again, in an even wider application, incompletely healed fractures are of interest in semiconductor device technology. The occurrence of "surface states" (i.e. energy levels within the forbidden energy gap characteristic of the bulk semiconductor) at such fracture interfaces leads to interesting electronic properties [8]. A complete understanding of these properties requires a quantitative knowledge of the "mismatch" that occurs across the fracture interface upon closure.

Ideally, in a study of crack closure and healing, one would like to be able to observe atom-on-atom mismatches across the interface. No *direct* methods yet exist for such a study, however, and at best one can only record *averaged* effects arising from a cumulative total of atomic mismatches (e.g. by measuring electronic properties). If, on the other hand, mismatch occurs over an extended array of atomic sites, as for instance in dislocations, stacking faults, voids, etc., one has available several standard techniques for making direct observations of any such deviations from perfect registry. Some of these techniques are capable of revealing certain aspects of small-scale mismatch with great sensitivity, as we shall show later.

In this article a study is made of the closure of Hertzian cone fractures in two highly brittle solids, glass and silicon. Hertzian fractures are preferred to more conventional types of fracture (e.g. cantilever fractures) because they are considerably easier to reproduce; indeed, several near-identical cone fractures can be made on the one specimen surface. Also, by suitably adjusting the loading cycle of the indenting sphere, the opening and closing of the cone crack interface can be controlled with relative ease. Further, the mechanics of cone crack growth in the solids chosen is well understood [9, 10], thereby providing a basis for a theoretical description of the various possible closure and healing mechanisms; this aspect is discussed in Section 2. From such theoretical considerations it is reasoned that the progress of the cone crack edge during a reloading stage should reflect any closure and healing that may occur at the fracture interface during the previous unloading stage. Accordingly a study of cone crack behaviour in a cyclic test is potentially capable of distinguishing between the various mechanisms postulated in Section 2. Glass, because of its transparency, is ideal as a medium for a study of this type; some optical observations of cone crack behaviour in glass are therefore presented in Section 3. However, while an optical examination provides a good deal of information concerning the fracture interface geometry over most of the crack length, it lacks the sensitivity required to reveal the configuration near the crack tip, where most closure and healing would be expected to occur. The highly strain-sensitive techniques of X-ray topography are better suited for an examination of the crack tip regions; consequently some complementary X-ray evidence of cone cracks in silicon is given in Section 4. The evidence obtained in both the optical and X-ray studies points to little closure or healing of the fracture interface during unloading of the specimen, with the closure prevention mechanism being purely mechanical in nature. Finally, it is pointed out that apart from macroscopic geometrical features the nature of the fracture process in the Hertzian test is essentially the same as in other tests, so that many of the observations presented here can be taken as representative of brittle fracture processes in general.

2. Theoretical Crack Closure and Healing Models

The loading of a hard, elastic sphere on the surface of a flat, elastic-brittle specimen solid produces initially a mutual elastic contact over a circle of radius a , according to the relation

$$a^3 = \frac{4k}{3E} P r, \quad (1)$$

where P is the normal load, r the sphere radius, E the Young's modulus of the specimen material, and k a dimensionless constant whose value (\approx unity) is a function of the elastic constants of both specimen and indenter [9]. Subsequent increase of the indenter load to a critical value P_c (corresponding to a critical contact radius a_c) initiates a cone-shaped fracture whose frustum intersects the specimen surface close to the circle of contact. Although equation (1) strictly derives from the assumption that the contact between indenter and specimen is purely elastic, it is found experimentally that no discontinuity occurs in this relation when cone fracture occurs: presumably this is because the specimen support for the indenter is imperceptibly diminished upon crack formation. It follows that optical measurements of the contact radius a may, via equation (1), be used as a calibration of the indenter load P throughout a Hertzian fracture test.

The mechanics of the growth of Hertzian fractures is somewhat complicated [9, 10], but a brief, qualitative picture of the process is sufficient to allow a distinction to be made between various possible types of crack closure behaviour. Essentially the cone crack initiates from a surface flaw, and propagates to a fully developed length, $\approx 3 a_c$, at which point a stable equilibrium is reached. The initiation may be spontaneous, or the flaw may first grow into a shallow stably propagating surface ring (to a depth of $\approx a_c/10$) before proceeding rapidly to full growth, depending on the original size of the flaw. This complication in the initiation stage is not readily detectable in an optical experiment ($a_c/10$ being typically some tens of microns), and will not lead to any confusion in interpretation in our experimental observations. Thus, based on theoretical considerations, our predicted sequence of observable events during loading is; (i) an increase in elastic contact to a critical radius a_c , (ii) a sudden unstable growth of the cone crack from a flaw to its ultimate development. This sequence is represented schematically by the stages labelled 1 and 2 in Fig. 1.

It is the manner in which the crack behaves on subsequent unloading and reloading of the specimen that determines the nature of the closure and healing at the interface. Three extreme possibilities are hypothesised in Fig. 1, and these now form the basis for the remainder of the discussion.

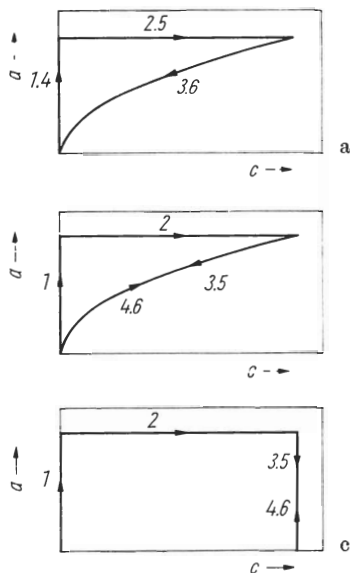


Fig. 1. Three hypothetical models, shown as plots of contact radius a against crack length c , representing extreme possibilities of cone crack behaviour on cyclic loading. a) Complete closure and perfect healing, b) complete closure but zero healing, c) zero closure and zero healing

a) *Complete closure and perfect healing of the crack.* If during the unloading stage (stage 3 in Fig. 1a)¹) the crack were to close completely and heal along its entire length it is evident that a second loading cycle, $4 \rightarrow 5 \rightarrow 6$, would exactly repeat the first, $1 \rightarrow 2 \rightarrow 3$. This implies complete reversibility in the fracture process which, in practice, can only be approached under unusually ideal conditions. Cleavage experiments on mica in ultra high vacuum (10^{-13} Torr) in which the crack front can be made to advance and retreat with little energy loss [12], and some controlled splitting experiments on silicon in similar vacuum [8], may be examples in which reversibility is very nearly achieved. In such circumstances atom-on-atom rebonding would require that no substantial rearrangement of unsaturated bonds occurs on a freshly cleaved surface.

However, even if the cone crack were to heal only partially on closure we might still expect to observe cyclic behaviour of the type depicted in Fig. 1a. A retreating crack would be expected to heal predominantly in the interfacial region close to the crack tip, so that a partially healed cone fracture would be characterised by a residual (unhealed) crack of length c_f (say). This residual crack would act effectively as the nucleating flaw for the second loading cycle. Provided that c_f be sufficiently small (less than $\approx a_c$ according to Hertzian fracture theory [9]) a threshold load (which might be somewhat smaller than for the first cycle) would again need to be exceeded in order that the cone fracture proceeds as before. A more exact treatment of this case would require a closer look at Hertzian fracture theory than we have presented here, but since the observations to be described later (Section 3) do not favour this model we will proceed no further with it.

b) *Complete closure but zero healing.* In this model (Fig. 1b) we allow the fracture interface to close completely (stage 3), thus relieving the residual elastic strain energy in the specimen, but prevent interatomic cohesive forces from acting across the interface. Thus the first loading cycle would proceed in a similar manner to that in case a), but upon reloading (stage 4), the crack would immediately begin to open up along the unloading curve (stage 3), the applied load no longer having to do work against cohesive forces at the fracture interface. Subsequent cyclic loading, $5 \rightarrow 6$ etc., simply releases and restores the elastic strain energy in the cracked specimen without hysteresis, thus retracing the same curve. This model implies the saturation of broken bonds on the freshly cleaved surface, either by a relaxation of surface atoms or by adsorption of a contaminant species. Referring again to previous work on mica, the presence of air at the cleavage interface leads to a substantial decrease in the inherent interfacial adhesion [4, 5], while the introduction of a fine layer of talc reduces the adhesion to a negligible level [6].

From the standpoint of cone fractures some authors (e.g. Benbow [13], working on fused silica) have observed that the interface can sometimes be made to disappear (optically) without trace on unloading. Whether in these cases the behaviour is more closely represented by the model in Fig. 1a or in Fig. 1b

¹) The unloading curve (stage 3) in Fig. 1a, 1b is plotted according to the analysis of Roesler [11], who showed that for $c \gg a_c$ the length of the cone crack could be made to increase stably with load P as $c \sim P^{2/3}$. Comparing this with equation (1) gives $c \sim a^2$. This relation, although not strictly valid for $c < a_c$, does satisfy the required condition that $c \rightarrow 0$ as $P \rightarrow 0$, so that it may be regarded as a useful first approximation to the theoretically expected behaviour in Fig. 1.

would require knowledge of the response of the crack to a reloading cycle. Further, a fracture interface in optical contact may well be separated by as much as several hundred angstroms (Section 3), in which case the behaviour would be more closely represented by model c).

c) *Zero closure and zero healing.* In this model the crack tip does not retreat upon release of the indenter load (stage 3 in Fig. 1c). Further cyclic loading, $4 \rightarrow 5 \rightarrow 6$, neither closes nor extends the crack length. This type of behaviour is supported by the optical observation of residual cracks in a majority of cases after Hertzian fracture tests on diamond and glass [14]. Since the elastic strain energy surrounding a cone fracture in a brittle solid can be reduced to zero only by removing the indenter and allowing the crack interface to close completely, the presence of a residual crack implies a closure prevention mechanism capable of withstanding substantial elastic restoring stresses. Such a mechanism, based on the wedging action of fracture "debris" at the closure interface, has been previously postulated [15].

Despite the implication of the residual crack observed *after* a Hertzian fracture test a cursory visual examination *during* such a test indicates that the crack edge does retreat (optically) to a certain extent. It is evident that a closer look at the fracture closure process is required if the applicability of any one of the above three models is to be asserted.

3. Optical Observations of Cone Fracture in Glass

The aim of the optical experiments was to provide data for comparison with the theoretical models outlined in the previous section. Observations were thus made of cone fracture behaviour, mainly in soda-lime glass, and to a lesser extent in fused silica. The chief difference between these two materials is that crack growth is considerably more time-dependent in glass. However, by allowing sufficient time between observations, thus allowing the cracks to approach their equilibrium lengths, this time-dependent effect proved no limitation in the following experiments. Glass, being the cheaper material, was thus favoured for a comprehensive study.

The experimental arrangement used for the optical studies is shown schematically in Fig. 2. The specimen, in the form of a plate glass slab 1/2 in. thick, was rigidly clamped on the stage of a metallurgical microscope. The indenter, a 1/2 in. diameter steel ball mounted in a specially constructed loading jig attached to the microscope stage, was then made to bear normally on the specimen surface. With this jig, an accurately machined double-screw system, the specimen could be loaded and unloaded at will, without any detectable rotation or lateral displacement of the indenter. The progress of the cone crack thus formed could be followed through the microscope.

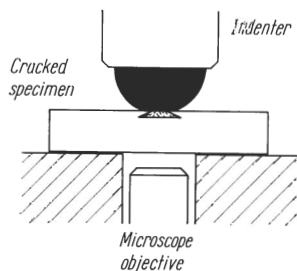


Fig. 2. Schematic diagram showing method of viewing cone crack under load

From the microscope examinations quantitative information could be obtained concerning the contact circle and fracture interface geometry. While the contact circle could be measured directly, the interface separation could only be inferred by means of its associated Fizeau fringe pattern (fringes of equal optical thickness, each successive fringe indicating a thickness change of one half wavelength of light). Since the accuracy with which the crack separations could be estimated depended to a large extent on the clarity and sharpness of this fringe system, much attention had to be given to obtaining the most favourable optical arrangements. With the low reflectivity of glass surfaces for visible light the fringe patterns resulted essentially from two-beam interference, thus precluding significant interference contrast from fracture surface detail much smaller than about one eighth of a wavelength of light (see [16, 17]). This immediately places a limitation on the accuracy with which the location of the crack tip can be determined.

3.1 Observations with polarized light

With light normally incident on the indented surface (Fig. 2) a faint image of the contact circle and the cone crack could be detected in reflection. The image contrast was found to be greatly enhanced by inserting a polarizer and analyser into the respective paths of the incident and reflected beams. The stress birefringence induced in the glass specimen (optically isotropic in the unstressed state) by the indenter led to partial transmission of the reflected beam when the analyser was in the crossed orientation. Extinction was observed to occur at those positions where the principal stresses in the radially symmetric Hertzian stress field were very nearly perpendicular to the transmission plane of either polarizer or analyser (dark cross region in Fig. 3).

Fig. 3 shows a typical sequence of observations during a loading and unloading cycle. In Fig. 3a the circle of elastic contact between indenter and specimen just prior to cone fracture occurring is shown (stage 1 in Fig. 1). In the original microscope image a set of closely spaced Newton's rings (corresponding to the air gap between indenter and specimen surface) surrounding the central dark patch could be clearly resolved. In Fig. 3b a cone crack is shown fully developed at critical load. The clearly visible surface trace of the cone (full circle) lies just outside the circle of contact (shown as broken circle). Surrounding the surface trace is a diffuse, concentric Fizeau fringe pattern. This is essentially a *transmission* interference pattern caused by normally reflected light from the upper surface of the specimen (Fig. 2) passing downward through the crack interface (inclined at some 20 to 25° to normal incidence) into the microscope objective. Micrographs c) and d) show two stages in the subsequent unloading of the specimen (stage 3 in Fig. 1). In these last two cases the stress birefringence is noticeably decreased.

Observations such as those in Fig. 3 permit, in principle, the motion of the cone crack to be followed as the circle of contact is made to expand and contract. However, while the movement of the crack walls can be estimated from the fringe pattern, the progress of the crack tip is more difficult to assess. For the location of the crack tip corresponds to the maximum in the zeroth order bright fringe, which is indistinguishable from the background illumination, and is therefore particularly difficult to assess with a system of only a few diffuse fringes. Nevertheless, the method provides an excellent optical means for qualitatively observing crack behaviour during cyclic loading. Thus in Fig. 3 the

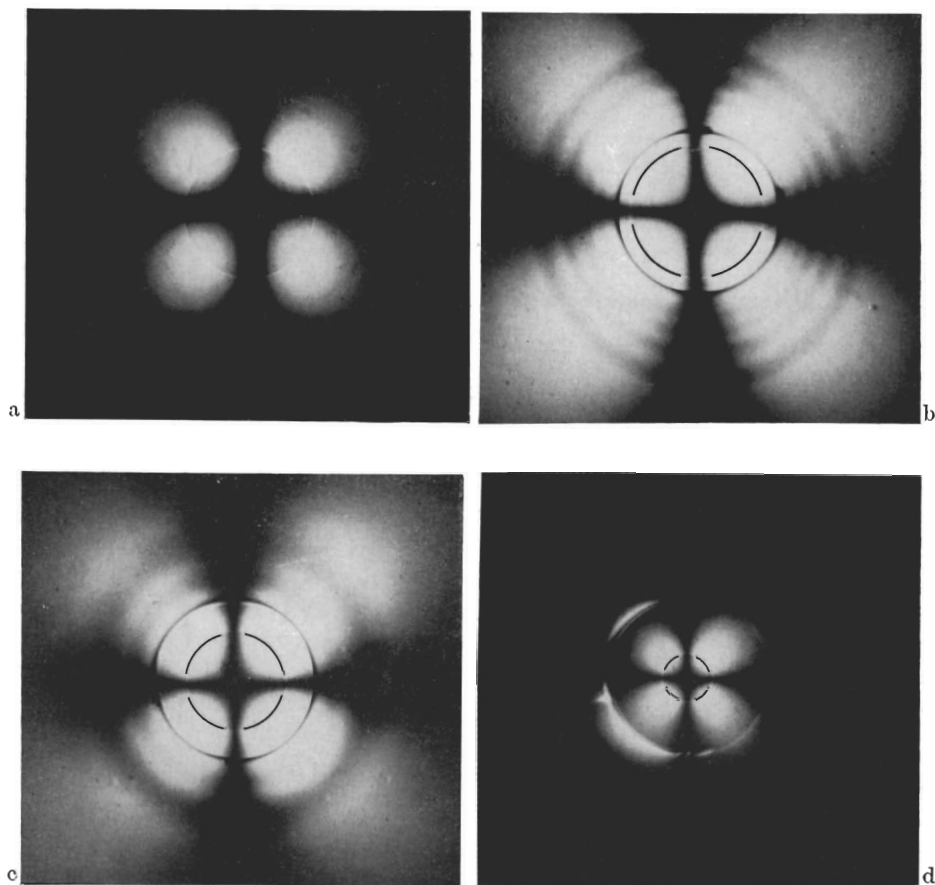


Fig. 3. Sequence viewed in reflected green light with crossed polars for a well formed cone crack. a) Elastic loading, b) crack formed at critical load, c) crack slightly unloaded, d) crack nearly completely unloaded. Micrographs b), c), and d) have been greatly underexposed relative to a) in order to emphasise the image of the fracture interface, to the detriment of the image of the contact circle: the latter is therefore artificially accentuated by means of the broken circles. Diameter of surface crack 640 μm

Fizeau fringe pattern is observed to contract on unloading, until at d) the fringes have disappeared and the crack separation is thus reduced to considerably less than one half of a wavelength of light. Further reduction of the load to zero (not shown in Fig. 3) resulted in almost complete extinction, with a small residual crack just detectable. Upon reloading (stage 4 in Fig. 1), the crack was observed to begin growing again immediately, and the sequence of patterns in Fig. 3 b, c, and d was almost exactly reproduced, in reverse order.

The observations described above reflect the general behaviour of hundreds of cone cracks examined in this way. In conjunction with the theoretical considerations in Section 2 these observations immediately lead to the rejection of the healing model, Fig. 1 a. More quantitative knowledge of the interface separation is required in order to distinguish between the two remaining possible models, Fig. 1 b and c.

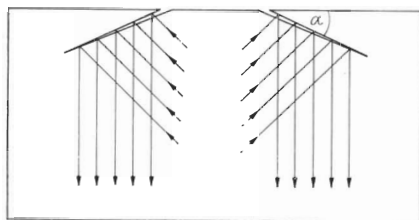


Fig. 4. Method of illuminating fracture interface with critically reflected oblique light. For glass $\alpha \approx 22^\circ$

3.2 Observations with critically reflected light

In order to view the cone fracture with greater clarity, critically directed oblique illumination was made to reflect specularly from the interface into the microscope objective²⁾ (Fig. 4). This condition was achieved by carefully directing light from a sodium lamp through the side walls of the glass specimen. Although only portions of the cone crack could be illuminated at any one time the image contrast was greatly improved, and the presence of structural features at the fracture interface could be clearly resolved. Moreover, the *reflection* interference pattern thus obtained showed sharper fringe minima. Fig. 5a indicates the quality of the image attainable, this being a reproduction of the cone

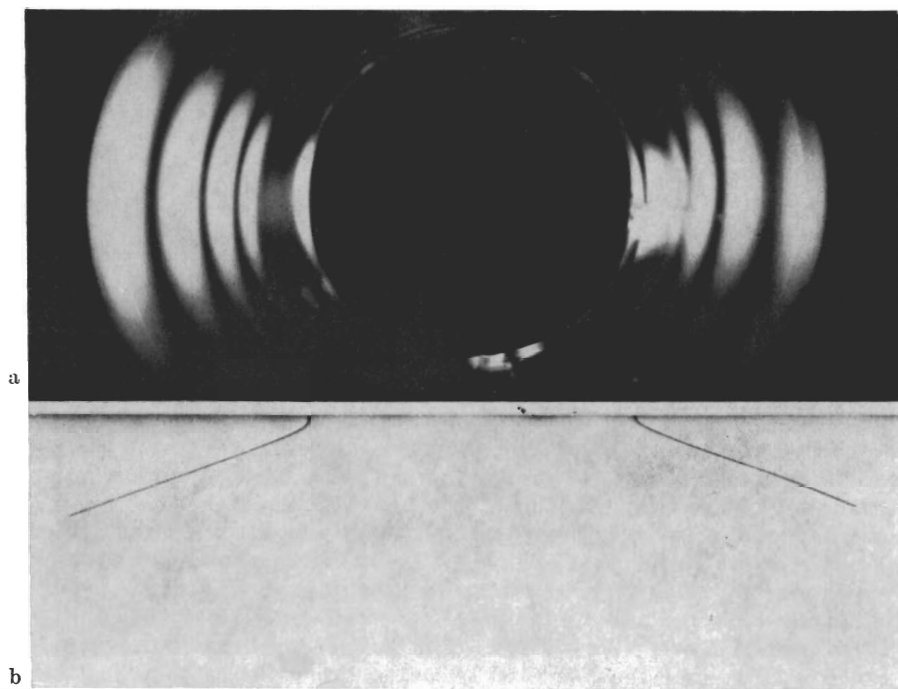
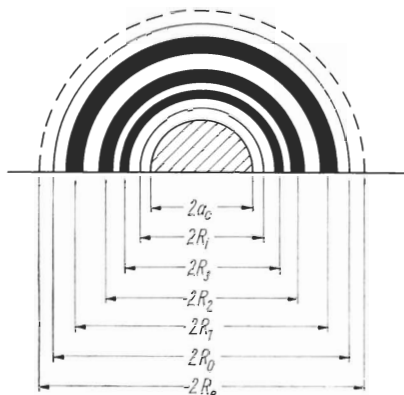


Fig. 5. a) Micrograph of the same crack as shown critically loaded in Fig. 3b, viewed here in critically reflected sodium light. Surface crack diameter 640 μm . b) Etched section of the same, unloaded crack

²⁾ An analogous optical arrangement has been used by Forty [18] to study cantilever cleavages in LiF.

Fig. 6. Schematic diagram showing manner in which the geometry of the optical crack is measured (see text)



crack at critical load shown previously in Fig. 3b. Although on unloading the clarity of this pattern deteriorated rapidly, the movement of both the fringe system and the optical crack edge could be more accurately followed than with polarized light. Under these conditions a semi-quantitative analysis of cyclic crack growth could be attempted.

Measurements of the cone crack geometry were thereby made according to the scheme in Fig. 6. The radial distances R were measured in the image plane from the centre of contact to the inner and outer edges of the optical (truncated) cone crack (R_i and R_o in Fig. 6), and to the dark fringes of m -th order (R_m ; $m = 1, 2, 3 \dots$ in Fig. 6). From the fringe measurements the crack separation profile could be determined at a given load by noting that the condition for destructive interference in reflection is that the optical path difference between incident and reflected beams be an integral number of wavelengths of light. Thus the crack separation t_m at the m -th order dark fringe follows from the relation

$$2 t_m (1 - n^2 \sin^2 \alpha)^{1/2} = m \lambda, \quad (2)$$

where n is the refractive index of the glass and α is the angle between the crack interface and the specimen surface (Fig. 4). Putting $n \approx 1.5$, $\alpha \approx 22^\circ$ (see [9],

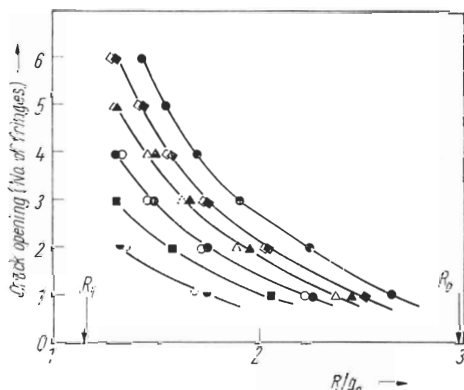


Fig. 7. Cone crack separation (plotted as fringe order) as function of radial distance for various stages of unloading (closed symbols) and reloading (open symbols) cycle. Curves shown correspond, in descending order, to $a/a_c = 1; 0.93; 0.88; 0.80; 0.70; 0.60$

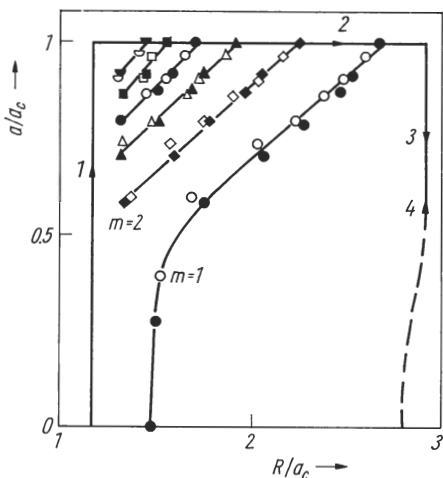
or Fig. 5b), equation (2) becomes

$$t_m \approx 0.43 m \lambda. \quad (3)$$

It is pointed out that despite the overall sharpening of the interference pattern in reflection the dark fringes still have finite width, so that there is still some degree of uncertainty associated with the precise location of the crack tip (i.e. $m = 0$ in equation (3)) ahead of the optically observable crack edge at R_0 .

A series of crack separation profiles was determined during unloading and reloading cycles for each of several cracks. Fig. 7 shows a family of plotted profiles for one of the less perfectly formed cone fractures (not the crack previously illustrated). Successively lower curves represent decreasing values of the contact radius a , which was measured at each stage of the loading cycle using the polarised light set-up (as in Fig. 3). The abscissa in Fig. 7 is normalised to the critical radius a_c , which determines the scale of the cone fracture. While the crack walls of this particular crack closed substantially during unloading, the outer edge of the optical crack at R_0 barely retracted from its original length at critical loading, although at low loads the poor image contrast rendered the crack edge almost invisible (the corresponding uncertainty in measurement is reflected by the dashed line in Fig. 8 below). An extrapolation of the curves in Fig. 7 to $t_m \rightarrow 0$ suggests that the crack tip lies a short distance ahead of R_0 , as one would expect. The data points in Fig. 7 also indicate that the same separation profiles are closely reproduced on reloading.

To facilitate a comparison of the experimental results with the theoretical models in Fig. 1 the data points in Fig. 7 are replotted in Fig. 8.³⁾ In this diagram the plotted points indicate the regression and expansion of the individual fringe minima. The continuous full lines (arrowed) indicate the following observed cycle: (i) the specimen is loaded elastically along stage 1, (ii) at the critical radius the cone crack initiates



just outside the circle of contact (stage 2), (iii) the optical crack edge retreats very slightly (stage 3). The results thus indicate that while the crack walls show a strong tendency to move together, they are somehow prevented from coming into close mutual contact. The theoretical model in Fig. 1c is thus favoured.

Fig. 8. Plot of a/a_c against R/a_c for the same crack depicted in Fig. 7. Data points indicate the contraction and expansion of individual fringe minima ($m = 1, 2, \dots, 6$) on unloading (closed symbols) and reloading (open symbols). The full line 1 \rightarrow 2 \rightarrow 3 \rightarrow 4 indicates the cyclic behaviour of the optical crack edge at $R = R_0$.

³⁾ The quantity $(R - R_i)/\cos \alpha$ corresponds very closely to the distance along the crack path. Thus the ordinate and abscissa in Fig. 8 bear very nearly a linear relationship with their counterparts in Fig. 1.

Although the results plotted in Fig. 7 and 8 represent the behaviour of a relatively imperfect cone fracture, the conclusions drawn above appear to be quite general. Even for those cone cracks which disappear optically on unloading, a subsequent examination of the indented specimen surface with two-beam fringe interferometry was sufficient to reveal the presence of a residual crack (cracks whose residual opening is as small as some tens of angstroms can be revealed in this way [14]). To investigate this point further the indented surfaces of some specimens were subjected to etching experiments. The most instructive information was obtained by sectioning cracked specimens normal to the indented surface, followed by carefully polishing down to the cone crack diameter, and finally etching in 5% HF for thirty seconds. In all cases a residual crack slightly longer than the length optically observable at full load was preferentially etched (R_c in Fig. 6). This is shown for the crack in Fig. 5, a crack specially selected for its conspicuous absence of interface imperfection. The observations of the residual cracks confirm that in no case does closure and healing occur over the optically detectable crack length, although no conclusion can be drawn as to any possible closure ahead of the etched crack edges.

3.3 Closure prevention mechanism

The results presented above suggest that the behaviour of cone cracks subjected to cyclic loading is best described by the theoretical model postulated in Fig. 1c. A closer inspection of the fracture interface indicates that the mechanism responsible for closure prevention is a purely mechanical one resulting from the inability of structurally complex fracture surfaces to key together on closure. With critically reflected light the presence of structural detail was clearly discernible at the interface in a vast majority of all cases studied. This detail was most commonly in the form of hackle lines and cleavage steps running in the direction of crack propagation, with some ripple-like markings concentric with the circle of contact evident at positions at which the crack was observed to stop (even in very slow growth). Such complexity of fracture markings is not uncommon [16, 19], and, indeed, examples of molecularly flat cleavages (e.g. as in carefully cleaved mica) are rare. Fig. 9, a portion of a cone crack interface viewed in critically reflected light at critical load, shows a typical cleavage step pattern. The ripple markings are less simple to photograph, but can be seen faintly within the outermost bright fringe in Fig. 5a.

Thus it seems highly probable that, in the likely event of some small lateral displacement across the interface occurring while the opposing faces are separated, the structural topography will prevent a mating of the fracture surfaces on closure. Indeed, in the most severe cases the structural imperfections may still be faintly detected after complete withdrawal of the indenter. It has, however, been pointed out that in very favourable circumstances, such as when opposing fracture surfaces do not completely disengage at full load, such surface structure might actually *enhance* closure by "guiding" the interface back to its original configuration [8]. On this basis it is argued that smaller cracks have a better chance of closing because their opposing fracture faces are less likely to become disengaged: this in turn implies a critical length (≈ 1 mm for small splits in silicon [8]) below which cracks might be expected to close. However, there is no evidence for such a "critical length" for cone cracks; in the study of natural diamond surfaces [20], for instance, naturally occurring residual cone fractures are observed down to some microns in size. It should also be pointed out that

cleavage step undercutting, leading to small cleavage fragments becoming dislodged [21, 22], is a common occurrence in brittle cleavages, and would further militate against the possibility of closure.

Other mechanisms for closure prevention are possible, but the present evidence argues strongly against their validity. Plastic flow, which plays an important role in healing prevention in alkali halides [18,23], has been previously presented as a possible mechanism in glass [24]. However, the same residual cracks are observed in diamond, which shows no evidence for any plasticity at room temperatures [15].⁴ Again, the possible effects of chemical contamination of the fresh fracture surfaces would appear to be insignificant in view of the wide residual crack openings often observed (sometimes exceeding several half wavelengths of light). Further, both plastic flow and chemical contamination would be expected to be rate-dependent effects, and careful inspection of several hundred residual cone cracks revealed no essential geometrical difference between those formed from static loading and those formed in an impact test [3] (similar results have been reported for germanium [25]).

The optical and etch study above has the important limitation that no conclusion can be made as to any possible crack closure and healing effects near the

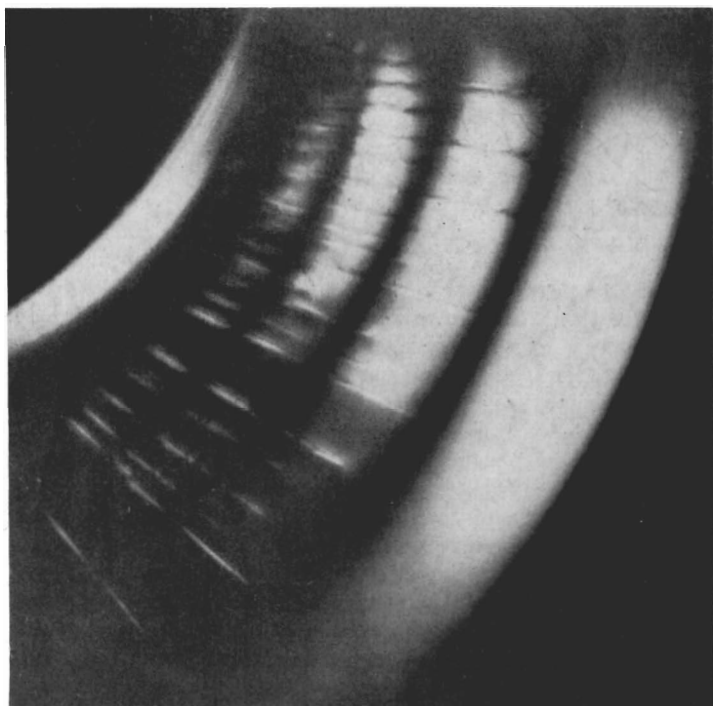


Fig. 9. Portion of a cone crack at critical load viewed in critically reflected light. Note presence of cleavage steps at interface. Width of field 600 μm .

⁴) The X-ray topographs presented later in Section 4 of this article further support this point; in none of the topographs is there any evidence of any dislocation mechanism associated with the residual cone cracks in silicon.

crack tip. Thus in Fig. 5 there must remain an element of uncertainty associated with the original full length of the cone crack; it could, for instance, be argued that the etchant is sensitive only to disturbances exceeding some minimum in severity, in which case a sufficiently well closed portion of interface may go undetected.

4. X-Ray Topographical Studies in Silicon

Since the insensitivity of the optical techniques used above preclude any definitive conclusion regarding the crack tip region where closure and healing are most likely to occur it is of interest to probe the residual crack interface with a more defect-sensitive technique. An X-ray diffraction topography investigation has therefore been made of the tip regions of residual cone cracks in silicon. X-ray topography [26] is a potentially powerful tool for such a study, being capable of clearly revealing defects of atomic mismatch (e.g. dislocations) in bulk specimens. Silicon is particularly suited to investigation by X-ray topography; slices of highly perfect single crystal can be selected to give high quality topographs with a low, featureless background intensity, so that any topographic detail observed in a cracked specimen may be unambiguously attributed to the presence of the crack. The one disadvantage of using silicon is that it is optically opaque, so that a direct comparison between optical and X-ray studies cannot be made. However, the geometry of the Hertzian fracture process in diamond structure crystals is very similar to that in glass [10, 15], with only a slight modification of the Hertzian cone arising from the (weak) tendency for cracks to follow the $\{111\}$ planes. The results presented in this section can therefore be regarded as complementary to those presented in Section 3.

4.1 X-ray topography of cracked specimens

Slices of silicon single crystal suitable for indentation testing were cut in the (111), (100), and (110) orientations. To avoid any danger of the specimens shattering during the testing procedure the slices were cut to an original thickness of 1 to 2 cm. The test surfaces were then mechanically polished, using finally 1 μm diamond paste, until a mirror finish was attained. The specimens were subsequently indented in a standard Instron testing machine, using a 1/2 in. tungsten carbide ball as indenter. Several Hertzian fractures were thereby produced on each test surface. The indented surfaces were then covered with a protective lacquer, and a thin surface slice sawn from the bulk specimen. The sawing damage on the underside of the surface slice was removed by mechanical abrasion, followed by a chemical polish in CP4, until the specimen was less than 1 mm thick. This procedure did not interfere with the cone cracks, and produced specimens suitable for X-ray examination.

Preliminary X-ray topographs taken of crystals prepared in the above manner showed intense diffraction contrast at the cone fracture sites. This contrast, attributable to the long-range elastic strain field surrounding the residual crack, completely obscured any detail within the crack tip region. A small layer of the indented surface was therefore polished away mechanically, and the specimen surface then given a light chemical polish to remove mechanical damage, in the hope that the upper, highly distorted regions of the residual cracks would be removed and a less obscured picture of the crack tip regions would be thereby

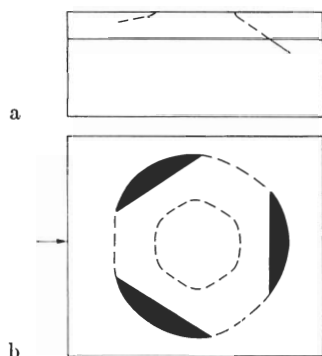


Fig. 10. a) Section view $[(101)$ plane] and b) plan view $[(111)$ plane] of cone crack in silicon. Dashed lines indicate portions of crack removed during preparation. Dark segments indicate portions of crack remaining. Arrows in b) indicate the section plane in a)

obtained. In all cases the topographic image quality was greatly improved. In particular, the specimens with (111) surfaces showed the most striking detail in image contrast: the subsequent discussion will therefore concentrate on this particular specimen orientation.

Fig. 10 shows schematically the fracture geometry for a (111) specimen prepared as above. In a) a section view of the cone crack is presented, and in b) a plan view. The surface trace of a cone crack on the (111) surface is a strongly rounded hexagon (inner dashed circle in Fig. 10b), from which the crack penetrates relatively deeply into the crystal on three alternate sides. The geometry of this crack therefore reflects the trigonal symmetry of the $[(111)]$ direction. In Fig. 10 the dashed lines represent portions of the crack removed by the surface polishing. This leaves, with a sufficiently heavy surface polish, only arcuate segments of crack (dark regions in Fig. 10) in the specimen. The surface traces of these segments were found to be delineated by etch lines arising from preferential etching in the CP4 solution.

A typical X-ray topograph of such a remanent crack is shown in Fig. 11. In this, as indeed in most cases, it is seen that the segments are not equal in size.

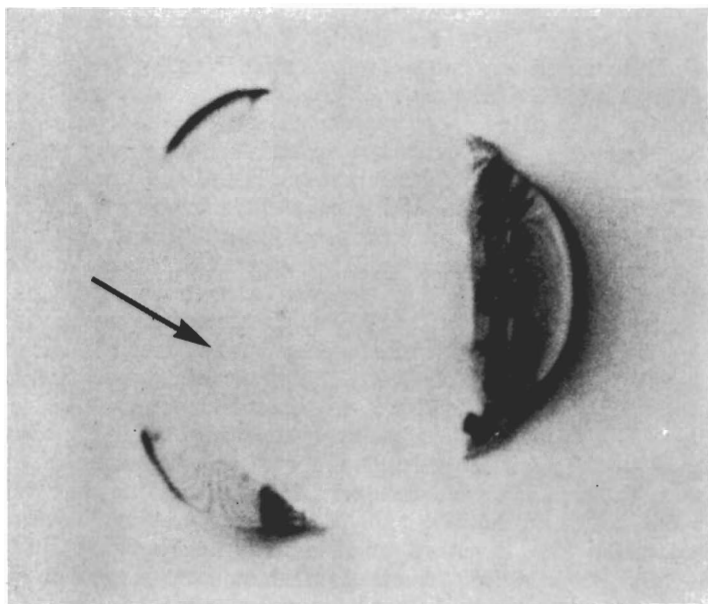
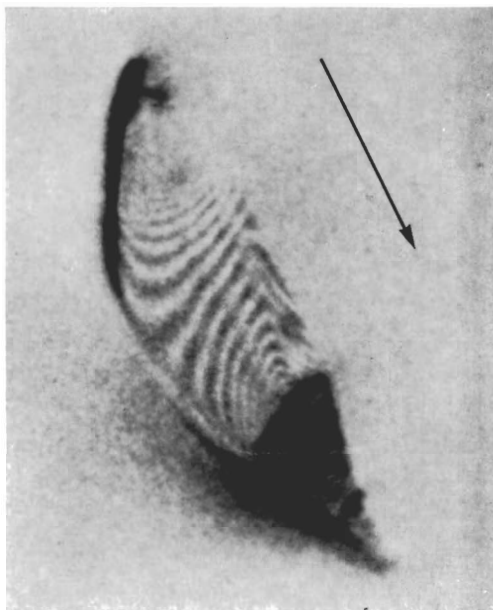


Fig. 11. X-ray topograph of specimen prepared as indicated in Fig. 10. 022 diffraction vector indicated. MoK α radiation

Fig. 12. Enlargement of crack segment at bottom-left in Fig. 11. Length of diffraction vector $250 \mu\text{m}$

This is attributable to slight deviations from normal loading of the indenter on the specimen surface [10]. Further, some cone cracks formed at higher critical loads than others, and consequently penetrated more deeply into the crystal. In such cases adjacent segments were not always completely separated from each other by the polishing procedure. Examples of these variants will appear in the next section.

It is clear in Fig. 11 that the surface polishing has removed any severe obscuring image contrast from the regions of crystal surrounding the fracture site. Some resolveable image detail is seen at the crack interfaces, including a prominent fringe pattern within the segment at bottom-left. This segment is shown enlarged in Fig. 12. The fringe pattern, and the other features of the X-ray image, will now be discussed in turn.



4.2 X-ray mismatch fringe patterns

Interference fringes in X-ray topographs of nearly perfect crystals have been ascribed to the following two sources: (i) Pendellösung interference between the dynamical wavefield components within the crystal, this manifesting itself as a system of equal thickness fringes. Such fringes are commonly observed at wedge-shaped crystal edges, and at internal low angle boundaries [26, 27]. We can, however, immediately reject this source in the present instance by noting that the fringes in Fig. 12 run very nearly perpendicular to the surface trace of the crack segment; fringes depicting equal thickness contours of the crystal wedge between crack interface and crystal surface would run very nearly parallel to this surface trace. (The fringe system in Fig. 12 is, nevertheless, faintly "modulated" at the Pendellösung depths [28]); (ii) mismatch interference between two simultaneously diffracting, adjacent portions of a crystal divided by an internal interface. Into this category fall the moiré fringe pattern, and the rigid body displacement fringe pattern. The moiré pattern is generated when the two overlapping crystals have a small mismatch in their periodic lattice spacing or lattice orientation. Moiré fringes have been previously observed at the interfaces of fortuitous cracks in natural quartz [28], as well as in other crystal superposition configurations [29 to 31]. The fringe systems arising from rigid body displacements of the crystal portions across the separation plane (hereafter termed *displacement* fringes) have more recently been found in ion implanted silicon [32, 33]. To distinguish between these two types of mismatch fringe systems we need to examine their individual diffraction properties.

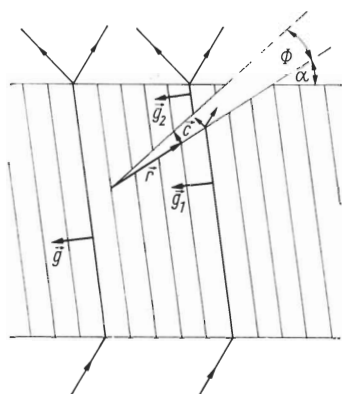


Fig. 13. Postulated deformation model for residual cone crack segment

In order to predict these diffraction properties we propose the residual crack model shown schematically in Fig. 13. In the most general deformation case originally coincident lattice planes undergo a rigid body displacement $\mathbf{c}(\mathbf{r})$ where \mathbf{r} is a position vector in the interface, and the diffracting planes adjacent to the interface have slightly different diffraction vectors, \mathbf{g}_1 and \mathbf{g}_2 . The angles Φ and α denote the angular separation of the crack walls (assumed constant) and the angle between crack interface and crystal surface ($\approx 35^\circ$) respectively; the crack angle Φ is grossly exaggerated, and in reality $\Phi \ll \alpha$. Since the Hertzian cracks open and close under the action of predominantly tensile stresses [10] we assume that the displacements \mathbf{c} are very nearly normal to the crack interface. We might also expect the plane of the diagram in Fig. 13 bisecting the crack segment to be a plane of symmetry for the deformation, but in view of the lack of symmetry in Fig. 11 this could prove to be a poor approximation.

The pure displacement fringe pattern arises when $\mathbf{c}(\mathbf{r})$ varies slowly with \mathbf{r} , with $\mathbf{g}_1 = \mathbf{g}_2 = \mathbf{g}$. The fringes are then loci [32] of

$$\mathbf{g} \cdot \mathbf{c} = \text{const.} \quad (4)$$

The fringes thus delineate contours of the displacement \mathbf{c} over the interface, the number of fringes increasing in proportion to the value of the constant in (4). For the diffraction conditions operating in Fig. 12 we have $\mathbf{g}(022) \cdot \mathbf{c} = 0$, so that no displacement fringes should appear. Further, since the internal boundary of the crack segment represents the contour $\mathbf{c} = 0$, no displacement fringes should intersect this boundary. Both these conditions are violated in Fig. 12.

Pure moiré patterns, on the other hand, arise when $\delta\mathbf{g} = \mathbf{g}_1 - \mathbf{g}_2 \neq 0$ [34], with \mathbf{c} having no varying component along \mathbf{g} . The fringes are then loci of

$$\delta\mathbf{g} \cdot \mathbf{r} = \text{const.} \quad (5)$$

The geometry of the crack segment does not restrict $\delta\mathbf{g}$ to zero in Fig. 12, so that a moiré system is not excluded. Accepting Fig. 12 as a moiré pattern we may determine the lattice distortion in the superposed crystals by means of the relation

$$\mathbf{G} = \delta\mathbf{g} = \mathbf{g}_1 - \mathbf{g}_2, \quad (6)$$

where \mathbf{G} is the reciprocal vector of the moiré system [34]. There are two types of moiré system, the dilation (or compression) moiré in which \mathbf{g}_1 and \mathbf{g}_2 differ

slightly only in magnitude (\mathbf{G} parallel to \mathbf{g}), and the rotation moiré in which \mathbf{g}_1 and \mathbf{g}_2 differ slightly only in direction (\mathbf{G} perpendicular to \mathbf{g}). Writing the spacings of the reflecting planes as $d = |\mathbf{g}|^{-1}$, $d_1 = |\mathbf{g}_1|^{-1}$, $d_2 = |\mathbf{g}_2|^{-1}$, and the spacing of the moiré fringes as $D = |\mathbf{G}|^{-1}$, we have for the two cases:

$$\frac{D}{d} = \frac{d}{|d_1 - d_2|}, \quad (\text{dilation}) \quad (7)$$

$$\frac{D}{d} = \frac{1}{\varepsilon}, \quad (\text{rotation}) \quad (8)$$

where $d_1 \approx d_2 \approx d$ for the dilation moiré, and $d_1 = d_2 = d$ with ε the angle between \mathbf{g}_1 and \mathbf{g}_2 for the rotation moiré. The left side of (7) and (8) represents the "moiré magnification" and the right side the inverse of the "lattice mismatch" of the superposed crystals. In Fig. 12 the fringe pattern is a mixture of the two types. With $d_{022} \approx 2 \text{ \AA}$ and the measured fringe spacing $D \approx 40 \text{ }\mu\text{m}$ in Fig. 12 a lattice mismatch of $\approx 5 \times 10^{-6}$ is calculated. Thus, according to (7) and (8) the fringes may be attributed to lattice spacing differences $d_1 - d_2 \approx \approx 10^{-5} \text{ \AA}$, and mutual lattice rotations $\varepsilon \approx 1''$. These figures vary by a factor of two or three either way for the many crack segments observed.

The above interpretation of the fringe systems in terms of a mismatch model may be confirmed by verifying the following two characteristic features of equations (4) and (5): (i) the fringe patterns are independent of the wavelength of the X-radiation, and (ii) the fringe patterns remain geometrically similar as the order of the reflection is changed, but change their spacing according to the relation $\mathbf{G}(nh, nk, nl) = n\mathbf{G}(h, k, l)$. Fig. 14 shows two adjoining crack segments exposed with $\text{AgK}\alpha$, $\text{MoK}\alpha$, and $\text{CuK}\alpha$ radiations; the geometry of the fringe pattern remains invariant, this verifying the first feature. (With $\text{CuK}\alpha$, however, the sign of the contrast is reversed, this being a common diffraction effect in crystals where X-ray absorption is high⁵.) The second feature has been checked by comparing 022 and 044 reflections. The fringe spacing in the latter reflection was found to be halved, as predicted; the visibility of the fringes was, however, very poor (see later), thus precluding photographic reproduction here.

In Fig. 12 and 14 above we have chosen our diffraction conditions such that only the moiré component of the mismatch fringe system remains in contrast. In other reflections, however, the displacement system will be expected to contribute. In Fig. 15 we show a series of topographs of another crack, exposed with $\text{AgK}\alpha$ radiation. The fringe geometry is seen to change markedly as the diffraction vector \mathbf{g} is varied. This observation conflicts with the prediction of equation (4), that the fringe pattern should be geometrically similar for all \mathbf{g} . On the other hand it is in keeping with the prediction of equation (5), that the fringe system should change as $\delta\mathbf{g}$ (which, in a general deformation configuration, is sensitive to \mathbf{g}) is varied. Using these two predictions as diagnostic criteria Bonse et al. [33] have shown that moiré or displacement components may be identified in those regions of the fringe pattern where one system is dominant.

⁵ In the dynamical diffraction of X-rays absorption is "high" or "low" according to whether μt is much greater than or less than unity, μ being the linear absorption coefficient and t the crystal thickness. In our experiments with silicon $t \approx 1 \text{ mm}$, so that $\mu t \approx \approx 0.8(\text{AgK}\alpha)$, $1.5(\text{MoK}\alpha)$, or $15(\text{CuK}\alpha)$.

On this basis we again conclude that our fracture interface patterns are predominantly moiré patterns.

It is unfortunate that any displacement component in Fig. 15 cannot be isolated, since this would give a pictorial indication of the crack separation profile. However, in the present case a rough evaluation of the crack angle Φ (Fig. 13) may be made by noting the fortuitous disappearance of fringe visibility as g becomes more closely perpendicular to the Φ -rotation axis, i.e. as the reflect-

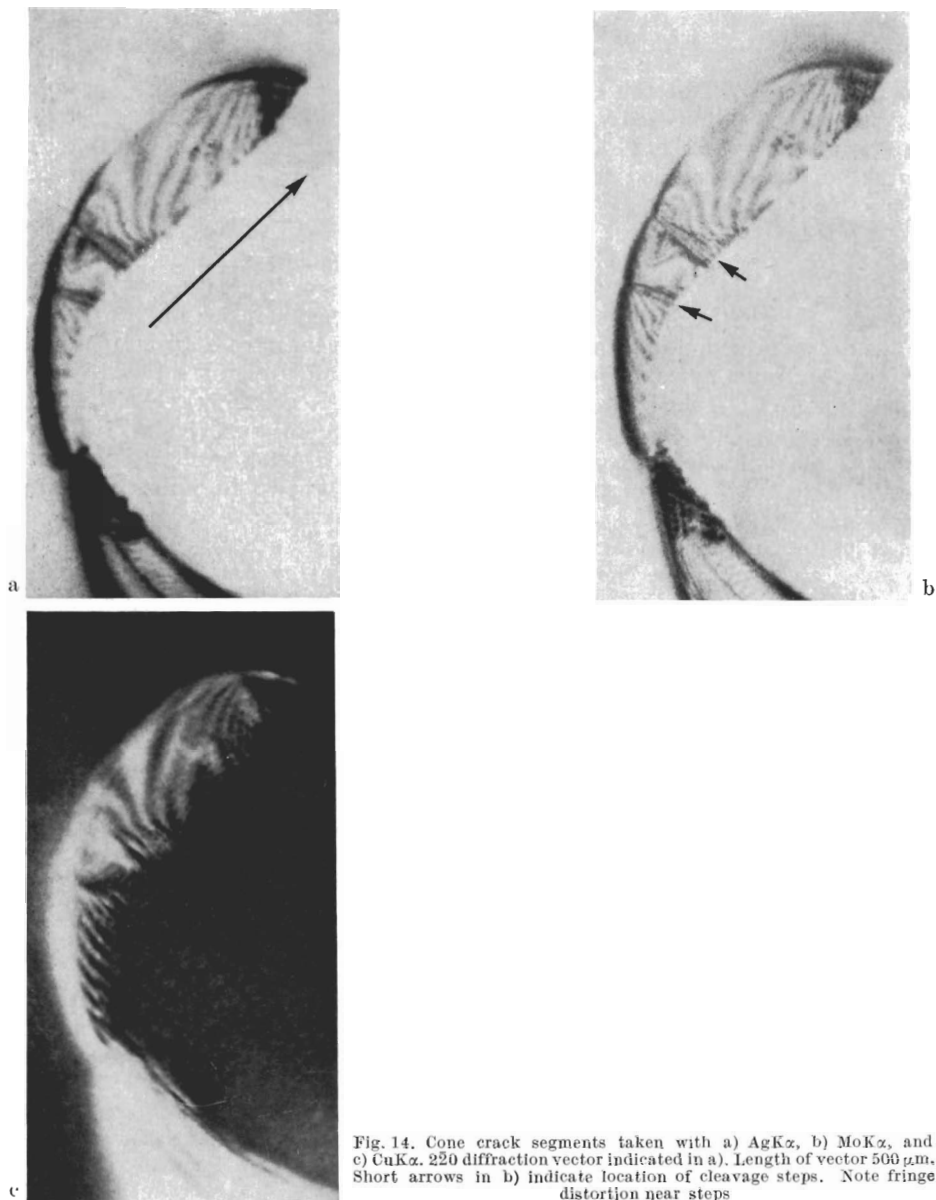


Fig. 14. Cone crack segments taken with a) AgK α , b) MoK α , and c) CuK α . 220 diffraction vector indicated in a). Length of vector $500 \mu\text{m}$. Short arrows in b) indicate location of cleavage steps. Note fringe distortion near steps

ing lattice planes on opposite sides of the crack interface suffer a greater component of the angular displacement caused by the displacement field $\mathbf{c}(\mathbf{r})$. This can be followed in the topographs shown here, noting in particular the near-disappearance of fringe contrast in the lower segment of Fig. 14 (seen best in the MoK α topograph) and the complete disappearance of fringe contrast in Fig. 15d. Now for mismatch fringe visibility to be high, the two overlapping crystal portions must simultaneously diffract the incident X-ray beam coherently. For this to occur the reflecting planes on opposite sides of the fracture interface should not be mutually misoriented by more than a half-width of the angular range of reflection of the perfect crystal [30]. The angular half-width for the 111 reflection using AgK α is 1.2×10^{-5} radians: thus if the crack angle Φ were to exceed this value, coherence would be lost under the diffraction conditions operating in Fig. 15d, and the absence of fringes thus explained. This conclusion is supported by the observation that fringe visibility also worsens systemat-

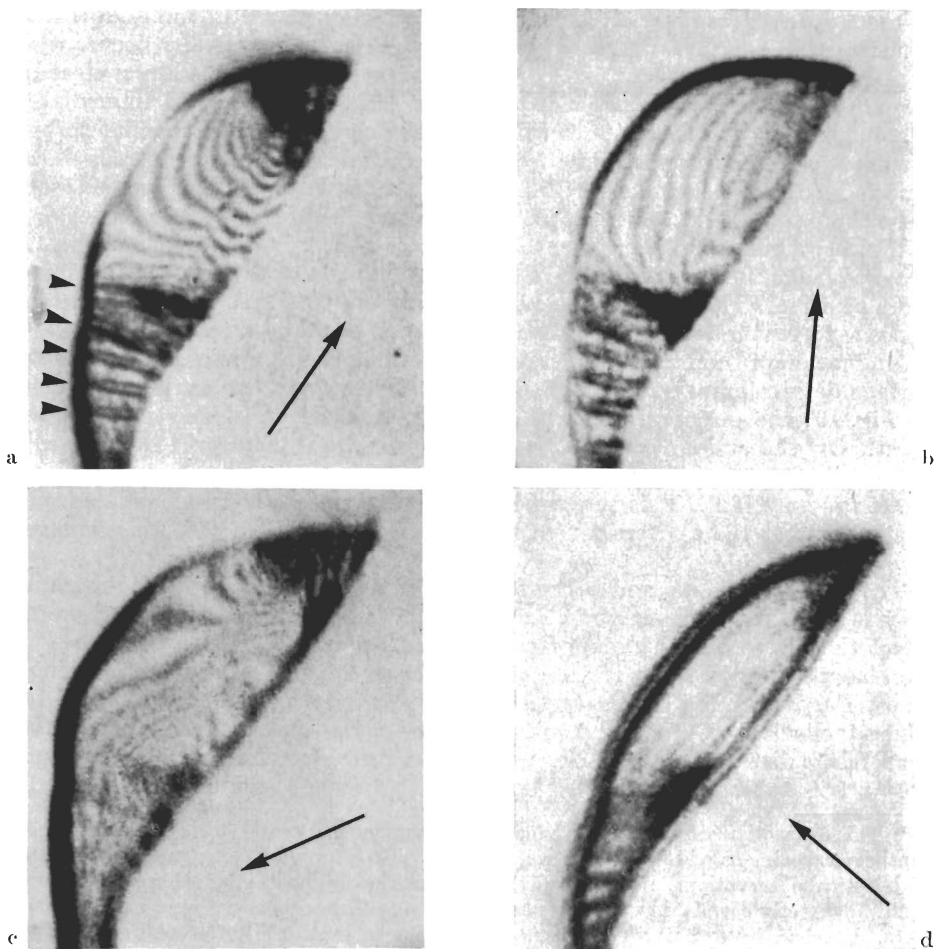


Fig. 15. Cone crack segment with a) $2\bar{2}0$, b) $1\bar{1}\bar{1}$, c) $1\bar{1}\bar{1}$, and d) $1\bar{1}\bar{1}$ reflections. Vector length $250 \mu\text{m}$. AgK α radiation. Short arrows in a) denote location of cleavage steps. Note disappearance of fringe contrast in d)

ically as higher order reflections are used (low index reflections having the largest angular half-widths). We conclude that $\Phi \approx (1 \text{ to } 5) \times 10^{-5}$ radians; for a crack segment $\approx 200 \mu\text{m}$ deep (e.g. Fig. 12) this corresponds to a residual crack mouth opening ≈ 20 to 100 \AA , which is commensurate with the optical observations in Section 3.

Thus an analysis of the fringe patterns yields a measure of lattice mismatch both transverse and normal to the crack segment interface. The cracks shown in the topographs are representative of dozens of examples studied. They have been selected not only because of their fringe patterns but also because of certain other prominent features in their topographic images which we now discuss in more detail.

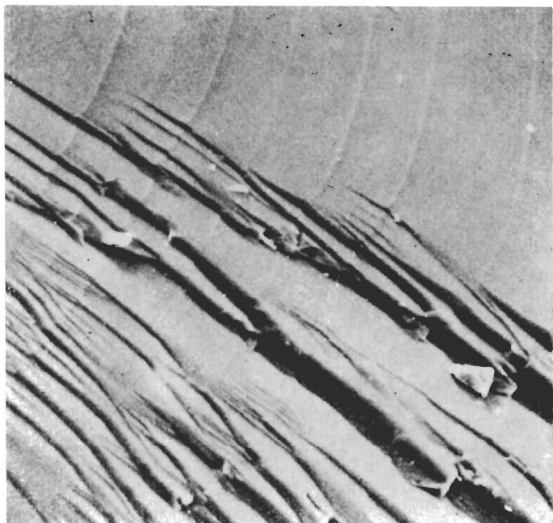
4.3 Closure prevention mechanism

A closer inspection of the topographs reveals the presence of cleavage steps and ripple markings within the crack interfaces. The cleavage steps, which run very nearly in the direction of crack propagation, are most readily discernible in the upper segment in Fig. 14, and in Fig. 15, by means of the double-lines of diffraction contrast. This type of contrast behaviour typically occurs when opposing fracture surfaces make contact only at the edges of the larger cleavage steps.⁶⁾ Moreover, the elastic displacement field in the crystal immediately surrounding such contact zones will only have significant components perpendicular to the cleavage step direction (plane strain), so that step contrast should tend to zero as g becomes more closely aligned with the step: this is indeed found to be the case in Fig. 15. A ripple marking is seen clearly in the lower segment in Fig. 14; it runs nearly parallel to the surface trace of the crack segment. In order to make the identification of these two features of the topographic image more positive we have polished down a freshly cracked specimen from the side *opposite* to that indented until the fracture cone could be extracted from below. Examination of the fracture surface in a scanning electron microscope revealed surface detail similar to that observed optically in glass. An example is shown in Fig. 16; the direction of crack propagation was from upper-left to lower-right. On the assumption that the ripple markings delineate the passage of the crack front it is clear that the cleavage steps have locally impeded the crack progress [22]. This pinning effect is also noticeable in the topographs, particularly at the two prominent steps at the interface of the upper segment in Fig. 14b.

That cleavage steps and other features of the fracture surface topography play a significant role in the closure prevention process is evident from the effect they have on the fringe patterns. In all cases the mismatch fringes are seen most clearly in those regions of interface separated by the more prominent steps. Further, the fringes are often grossly distorted near the steps (e.g. Fig. 14), where the lattice distortion would be expected to be most severe. In some other cases fringe distortion was observed at localised regions of severe strain, presumably attributable to pieces of dislodged fracture debris; this is seen in Fig. 17.

⁶⁾ This diffraction effect has been more clearly analysed in partially cleaved transparent cantilever specimens of LiF [35], in which X-ray diffraction effects are readily correlated with optical observations. For these LiF specimens the double lines of diffraction contrast could be directly correlated with the mutual contact of large steps on opposing crack surfaces. Further, by examining the residual cleavage interfaces in reflected light [18] the presence of optical interference fringes clearly indicated that the crack walls were separated between the contacting steps.

Fig. 16. Scanning electron micrograph of extracted cone crack surface. Crack propagated from upper-left to lower-right. Note ripple markings (arc-like traces), cleavage steps, and pieces of dislodged fracture "debris". Width of field 350 μm



A few examples were found in which the fracture interface showed almost no detectable fracture markings. In these instances (e.g. Fig. 18) the fringe spacing was wide, indicating a small lattice mismatch.

It was argued in Section 4.2 that the variation of fringe visibility with change of reflecting plane was consistent with a small angular separation of the walls of the residual crack. This implies a residual strain concentration in the vicinity of the crack tip, hence explaining the enhanced diffraction contrast observed in this region in all the topographs. In a manner similar to that for the cleavage steps the contrast vanishes at those points where g becomes aligned with the crack front (see especially Fig. 15).

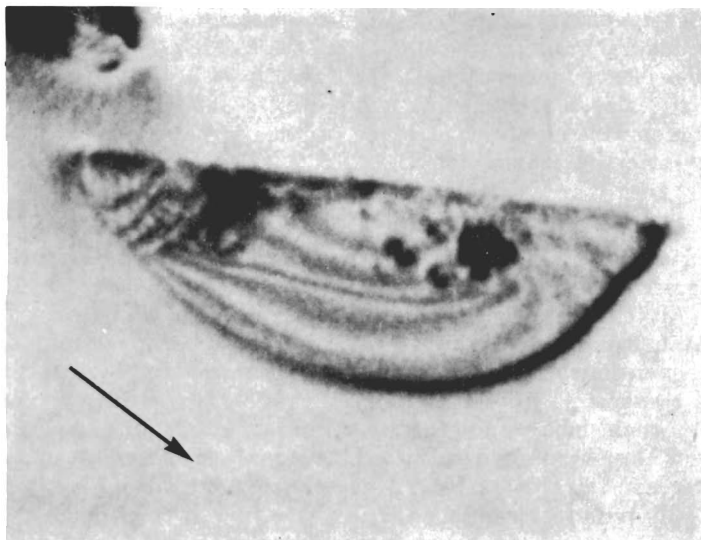


Fig. 17. Topograph of crack segment, showing fringe distortion at regions of localized strain. $\bar{1}\bar{1}\bar{1}$ reflection. AgK α radiation. Vector length 250 μm

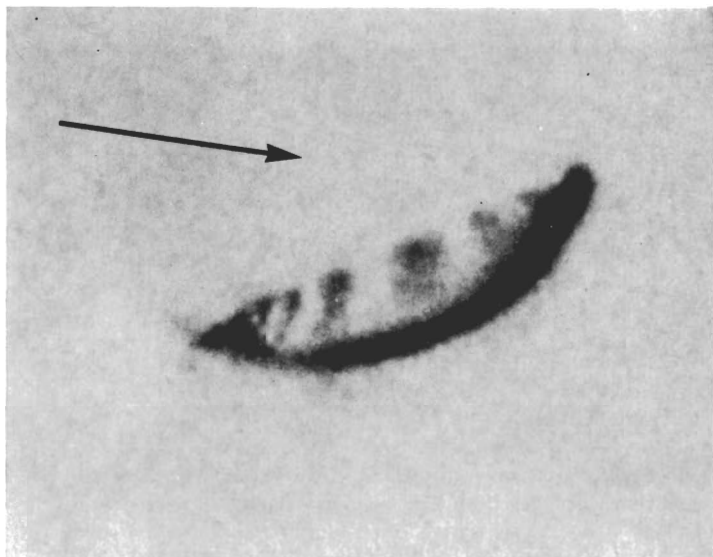


Fig. 18. Small segment relatively free from interfacial fracture markings. $\bar{1}\bar{1}\bar{1}$ reflection. AgK α . Vector length 250 μm

An important feature of the topographic images was that the crack tip region appeared to be very clearly delineated in all crack segments studied. In no case was there any evidence that the crack front had ever proceeded beyond the region visible in the topographs; had the crack penetrated further it would seem likely that *some* unhealed regions, particularly in the vicinity of the larger cleavage steps, would be apparent. The absence of any such regions strongly suggests that within the limit of resolution of the topographic method (a few microns) no healing or closure occurs at all. It is, nevertheless, pointed out that the residual mismatch at the crack interface is small, typically on an angstrom scale, so that healing might conceivably be induced by artificial means in favourable circumstances. e.g. by heating or by applying a suitable compressive stress to the specimen.

5. Conclusion

The observations presented above strongly favour the hypothesis that neither healing nor significant mutual recontact occurs across the detectable cone crack interface. Although the fracture geometry generally changes from glass to single crystal, from crystal surface to crystal surface, and from cone crack to more conventional fracture testing arrangements, the surface topography apparently responsible for the closure prevention is typically the same in all cases. Our conclusions would therefore appear to be quite general. Indeed, moiré fringes have been observed near cleavage steps at the interfaces of cantilever cleavages in LiF crystals [35]. It is clear that optical and X-ray techniques are potentially powerful tools for the investigation of crack healing behaviour down to an atomic scale for fracture geometries other than the one discussed here.

Acknowledgements

We wish to thank Dr. D. B. Holt for criticisms of the manuscript. Mr. P. Felton took the scanning electron micrograph (Fig. 16). The receipt of Commonwealth Scholarships (JSW and MVS) is gratefully acknowledged.

References

- [1] B. R. LAWN, Proc. Roy. Soc. **A299**, 307 (1967).
- [2] R. E. MOULD, Fundamental Phenomena in the Materials Sciences, Eds. L. J. BONIS, J. J. DUGA, and J. J. GILMAN, Plenum Press, New York 1967 (p. 119).
- [3] F. B. LANGITAN and B. R. LAWN, J. appl. Phys. **40**, 4009 (1969).
- [4] J. W. OBREIMOFF, Proc. Roy. Soc. **A127**, 290 (1930).
- [5] E. OROWAN, Z. Phys. **82**, 239 (1933); **82**, 259 (1933).
- [6] F. P. BOWDEN and D. TABOR, The Friction and Lubrication of Solids, Part II, Chap. 20, Oxford University Press, 1964.
- [7] F. B. LANGITAN and B. R. LAWN, to be published.
- [8] D. HANEMAN, W. D. ROOTS, and J. T. P. GRANT, J. appl. Phys. **38**, 2203 (1967).
- [9] F. C. FRANK and B. R. LAWN, Proc. Roy. Soc. **A299**, 291 (1967).
- [10] B. R. LAWN, J. appl. Phys. **39**, 4828 (1968).
- [11] F. C. ROESLER, Proc. Phys. Soc. **B69**, 981 (1956).
- [12] P. J. BRYANT, L. H. TAYLOR, and P. L. GUTSHALL, Trans. 10th National Vacuum Symp., Macmillan, New York 1963 (p. 21).
- [13] J. J. BENBOW, Proc. Phys. Soc. **75**, 697 (1960).
- [14] V. R. HOWES and S. TOLANSKY, Proc. Roy. Soc. **A230**, 287 (1955); **A230**, 294 (1955).
- [15] B. R. LAWN and H. KOMATSU, Phil. Mag. **14**, 689 (1966).
- [16] S. TOLANSKY, Surface Microtopography, Longmans, London 1960.
- [17] L. HOLLAND, The Properties of Glass Surfaces, Chap. 2, Chapman and Hall, London 1964.
- [18] A. J. FORTY, Proc. Roy. Soc. **A242**, 292 (1957).
- [19] C. A. ZAPFFE and C. O. WORDEN, Acta cryst. **2**, 377 (1949); **2**, 383 (1949); **2**, 386 (1949).
- [20] S. TOLANSKY and A. HALPERIN, Proc. Phys. Soc. **B67**, 473 (1954).
- [21] J. D. VENABLES, J. appl. Phys. **31**, 1503 (1960).
- [22] F. F. LANGE, and K. A. D. LAMBE, Phil. Mag. **18**, 129 (1968).
- [23] A. J. FORTY and C. T. FORWOOD, Trans. Brit. Ceram. Soc. **62**, 715 (1963).
- [24] D. M. MARSH, Proc. Roy. Soc. **A279**, 420 (1964).
- [25] E. N. PUGH and L. E. SAMUELS, Phil. Mag. **8**, 301 (1963).
- [26] A. R. LANG, J. appl. Phys. **30**, 1748 (1959).
- [27] N. KATO and A. R. LANG, Acta cryst. **12**, 787 (1959).
- [28] A. R. LANG and V. F. MIUSCOV, Appl. Phys. Letters **7**, 214 (1965).
- [29] J. CHIKAWA, Appl. Phys. Letters **7**, 193 (1965).
- [30] A. R. LANG, Nature **220**, 652 (1968).
- [31] U. BONSE and M. HART, Z. Phys. **190**, 455 (1966).
- [32] U. BONSE and M. HART, phys. stat. sol. **33**, 351 (1969).
- [33] U. BONSE, M. HART, and G. H. SCHWUTTKE, phys. stat. sol. **33**, 361 (1969).
- [34] R. GEVERS, Phil. Mag. **7**, 1681 (1962).
- [35] C. T. FORWOOD and B. R. LAWN, unpublished work.

(Received February 9, 1970)

Note added in proof:

Since submitting this article some recent work by S. M. Weiderhorn and P. R. Townsend (private communication) has been made available to us. By following double-cantilever cracks optically in soda-lime glass slides these authors have apparently been able to establish partial crack reversibility under favourable test conditions.